Polarization-stiffened ferroelectric liquid crystals: A thickness-independent bistable switching voltage with a lower limit of about 2 V and the transition to thresholdless switching

Michael J. O'Callaghan*
964 West Maple Court, Louisville, Colorado 80027, USA
(Received 27 August 2014; revised manuscript received 18 November 2014; published 23 February 2015)

Typical ferroelectric Sm-C^* liquid crystal (FLC) cells exhibit a voltage threshold for switching from one stable state to another despite the FLC's response being inherently continuous and thresholdless (free rotation of the director around the tilt cone). This switching threshold is due to FLC-surface interactions and to the chevron smectic structure commonly formed in cells. It is shown here that the FLC electrostatic energy contribution $\sim {P_S}^2$ responsible for thresholdless switching of high-P_S FLCs also plays a key role in the bistable switching of lower-P_S FLCs. Among the consequences are that it can be difficult to lower a cell's threshold below $V_{TB} \sim 3.4(B/\varepsilon_F)^{1/2}$ (B and ε_F are the FLC's elastic and dielectric constants), that a cell's threshold becomes independent of cell thickness once it substantially exceeds the characteristic length $\xi_P = (\varepsilon_F B)^{1/2}/P_S$, and that there are conditions under which alignment layer capacitance can decrease rather than increase the threshold (i.e., transition to thresholdless switching). A model that predicts and explains these behaviors is presented along with threshold measurements of representative FLC cells.

DOI: 10.1103/PhysRevE.91.022502 PACS number(s): 61.30.Dk, 42.79.Kr, 61.30.Eb, 61.30.Hn

I. INTRODUCTION

Although the response of a Sm-C^* ferroelectric liquid crystal (FLC) to an electric field is inherently thresholdless (free rotation of the director around the tilt cone), surface-stabilized FLC (SSFLC) *cells* typically exhibit bistability. Bistability arises from the interaction between FLC properties, cell surfaces, and the usually present chevron structure (e.g., giving rise to up and down domains) [1]. The strength of interactions at cell surfaces and at the chevron interface (boundary between layers of differing tilt) of course plays an important roles in determining a cell's threshold voltage $V_{T\text{cell}}$ for bistable switching. Here we investigate the influence, which can be large, of additional FLC and cell properties on the threshold.

This work was undertaken with the aim of understanding why, in Displaytech's[1] experience, it was difficult to achieve thresholds of less than about 2 V despite exploring a wide range of FLC and alignment surface types. This investigation also unexpectedly provides insight into the transition from bistable to thresholdless switching that occurs as FLC and cell parameters are varied (e.g., as polarization or alignment layer thickness are increased).

Due to FLC cells' well-known bistability, it was of great interest when examples of thresholdless switching were discovered [2–4]. Subsequent investigations found that, in general, FLCs having a large spontaneous polarization P_S ($\gtrsim$200 nC/cm^2) can be expected to exhibit thresholdless switching due to an electrostatic energy contribution proportional to P_S^2, which stiffens the director structure and overwhelms surface influences [5–8]. Here it is shown that polarization stiffening also plays an important role in bistable switching of lower polarization FLCs. Two important consequences are that (i) the FLC threshold voltage V_{TF} (voltage across the FLC layer only) becomes independent of FLC layer thickness L_F once it substantially exceeds the characteristic length $\xi_P = (\varepsilon_F B)^{1/2}/P_S$ (B is the director rotation elastic constant) and (ii) there is a limiting voltage $V_{TB} \sim 3.5(B/\varepsilon_F)^{1/2}$ below which it becomes harder to further reduce V_{TF} by increasing P_S or by reducing the surface anchoring energy.

Dielectric alignment layers are capacitances in series with the FLC and their presence would in general be expected to raise a cell's switching threshold $V_{T\text{cell}}$ above that of the FLC layer alone (V_{TF}). Here this is found to be true for FLC layers having $V_{TF} > V_{TB}$, but for $V_{TF} < V_{TB}$ it is found that increased alignment layer thickness can either raise or lower a cell's switching threshold depending on B and details of the surface interaction energy. Related to this, it is shown that alignment layers can degrade bistability if their thickness is comparable to or exceeds the characteristic length ξ_P. In this thickness range a transition from bistable to thresholdless switching occurs, consistent with previous models of thresholdless switching [5–8]. It is also seen that a Frederiks-like threshold $V_{\text{Fred}} = \pi^2 B/P_S L_F$ may exist under certain conditions.

This investigation begins with a bookshelf smectic layer model. A mathematical approach was devised in which numerical calculations of switching thresholds are used to map out the range of cell behaviors and then approximate analytical solutions of the nonlinear equations are used to identify key relationships. The effects of alignment layer capacitance and chevrons are then included. Finally, measurements of representative bistable FLC cells are presented for comparison with the model and in particular to test the prediction of a thickness-independent threshold voltage.

*email.mocallaghan@gmail.com

[1]Displaytech was acquired by Micron Technology after completion of the experimental work and is now owned by Citizen Finetech Miyota.

II. MODEL

The bookshelf FLC cell model is illustrated in Fig. 1 where source V drives charge Q onto the series capacitances. We

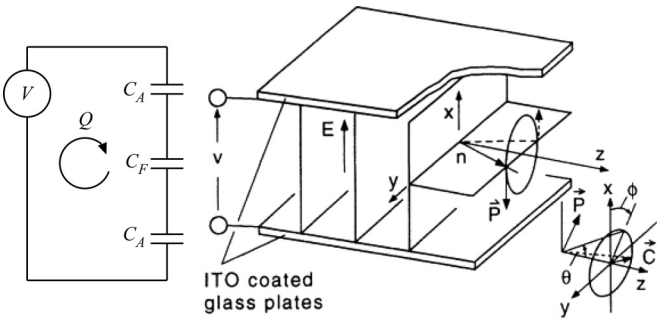

FIG. 1. In this circuit model C_A and C_F represent alignment layer and FLC layer capacitances. The illustration [2] of bookshelf smectic layers within a cell shows the coordinate system used in the model.

could write down the Lagrangian (including dissipation terms making the connection to free energy and thermodynamics) and then use Hamilton's principle to determine the governing time-dependent differential equations. Here, however, we are only concerned with static equilibrium solutions and so need only to find minima of the combined elastic and electrostatic potential energies U [Eq. (1)]. We first consider the FLC layer and its surface interactions alone, driven by charge Q. For the elastic plus electrostatic energy density u we use the simplest model known to reproduce the main features of typical SSFLC cells

$$u = \frac{1}{2}B\left(\frac{d\varphi}{dx}\right)^2 + \frac{1}{2}\varepsilon_F|\mathbf{E}|^2,$$
$$\mathbf{E} = -\frac{1}{\varepsilon_F}\left(\frac{Q}{A} + \mathbf{P}\cdot\hat{\mathbf{x}}\right)\hat{\mathbf{x}}, \quad \mathbf{P} = P_S(\cos\varphi\hat{\mathbf{x}} + \sin\varphi\hat{\mathbf{y}}),$$
$$U = \int_0^{L_F} u dx + w_0(\varphi)|_{x=0} + w_L(\varphi)|_{x=L_F}. \tag{1}$$

Here A is the cell area, $P_S > 0$, and w_0 and w_L are surface interaction energy densities. A positive charge Q on the electrode at $x = L_F$ (with $-Q$ at $x = 0$) generates an electric field pointing in the $-x$ direction. The corresponding Euler-Lagrange equations governing steady-state equilibrium solutions for dipole orientation $\varphi(x)$ are found by the usual method of calculus of variations [9]

$$\frac{d^2\varphi}{dx^2} + \left(\frac{\mathrm{sgn}(q)}{\xi_{PE}^2} + \frac{1}{\xi_P^2}\cos\varphi\right)\sin\varphi = 0, \tag{2a}$$

$$\left(B\frac{d\varphi}{dx} - \frac{\partial w_0}{\partial\varphi}\right)\Big|_{x=0} = 0,$$
$$\left(-B\frac{d\varphi}{dx} - \frac{\partial w_L}{\partial\varphi}\right)\Big|_{x=L_F} = 0, \tag{2b}$$

$$\xi_P = \frac{\sqrt{\varepsilon_F B}}{P_S}, \quad \xi_{PE} = \sqrt{\frac{B}{P_S|E_Q|}},$$
$$E_Q = -\frac{q}{\varepsilon_F}, \quad q = \frac{Q}{A}. \tag{2c}$$

From combining expressions in Eqs. (2c) it can be seen that the ratio $|q|/P_S$ dictates which length scale is smallest,

$$|q|/P_S > 1 \leftrightarrow \xi_P > \xi_{PE},$$
$$|q|/P_S < 1 \leftrightarrow \xi_P < \xi_{PE}. \tag{3}$$

In dimensionless form the Euler-Lagrange equations are

$$\frac{d^2\varphi}{d\tilde{x}^2} + (\tilde{q} + \cos\varphi)\sin\varphi = 0,$$
$$\left(\frac{d\varphi}{d\tilde{x}} - \frac{\partial\tilde{w}_0}{\partial\varphi}\right)\Big|_{\tilde{x}=0} = 0, \quad \left(-\frac{d\varphi}{d\tilde{x}} - \frac{\partial\tilde{w}_L}{\partial\varphi}\right)\Big|_{\tilde{x}=\tilde{L}} = 0,$$
$$\tilde{x} \equiv x/\xi_P, \quad \tilde{q} \equiv \frac{q}{P_S},$$
$$\tilde{w}_0 = \frac{\xi_P}{B}w_0, \quad \tilde{w}_L = \frac{\xi_P}{B}w_L, \quad \tilde{L} = \frac{L_F}{\xi_P}. \tag{4}$$

Once alignment layers are included the ratio of ξ_P to alignment layer thickness is also important (Secs. V and V C). The voltage V across the FLC cell is related to both the charge Q and the spatially varying dipole orientation $\varphi(x)$,

$$V = \left(\frac{2L_A}{\varepsilon_A} + \frac{L_F}{\varepsilon_F}\right)\frac{Q}{A} + \frac{P_S}{\varepsilon_F}\int_0^{L_F}\cos\varphi dx. \tag{5}$$

It is useful to define low, medium, and high polarization according to ratios of the characteristic stiffening length ξ_P to the FLC and alignment layer thicknesses (Table I). The FLC layer thickness is commonly chosen to obtain half-wave optical retardation; typical values are around 1 μm for use in reflection or 2 μm for transmission. Typical alignment layer thicknesses are ~20 nm. The focus here is on medium-P_S FLCs (~10−100 nC/cm^2) since these should generally exhibit the lowest switching thresholds short of becoming thresholdless at higher-P_S values.

TABLE I. Definition of approximate FLC polarization ranges. The P_S ranges are calculated using representative values of $B =$ 10 pN, $\varepsilon_F = 4\varepsilon_0$, $L_F \cong 1$−$2\,\mu$m, and $L_A \cong 20$ nm.

P_S category	Criteria	P_S range
low	$\xi_P > \frac{1}{4}L_F$	<10 nC/cm^2
medium	$L_A < \xi_P < \frac{1}{4}L_F$	10−100 nC/cm^2
high	$\xi_P < L_A, \xi_P = L_F$	>100 nC/cm^2

Interactions between cell surfaces and the FLC are represented by an anchoring energy function $w(\varphi_S)$, where φ_S is the dipole orientation at the surface. A simple example of a bistable surface interaction energy [1] is (Fig. 2)

$$w(\varphi_S) = -\gamma(\mathbf{P}\cdot\hat{\mathbf{n}}_S)^2 = -\gamma\cos^2\varphi_S \tag{6}$$

This nonpolar example has equal minima at $\varphi_S = 0°$ and 180° (dipole pointing either into or out of the surface). Here $\hat{\mathbf{n}}_S$ is the surface normal pointing along the x axis at $x = 0$ and opposite the x axis at $x = L_F$. Representative values of γ (e.g., on a polyimide) are reported to be [10] on the order of 1 erg/cm^2.

The torque density applied to the FLC by the surface is $-dw/d\varphi_S$. For the surface energy example of Eq. (6), surface torque maxima $N_M = \pm\gamma$ occur at $\varphi_S = \varphi_M = 45°$ and 135°. Regardless of the specific form of the surface energy

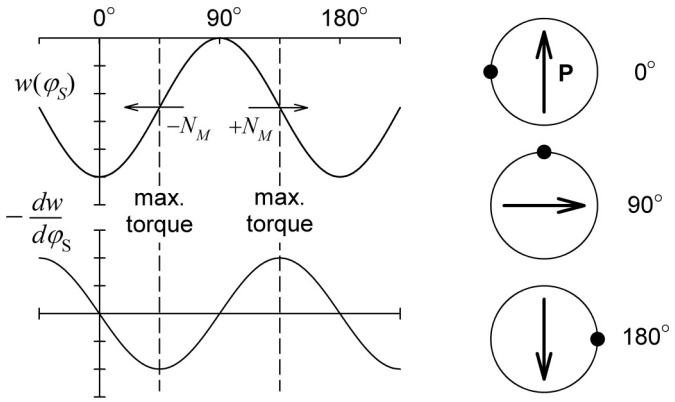

FIG. 2. Shown on the left is the model surface interaction energy $w(\varphi_S) = -\gamma\cos^2\varphi_S$ and torque $N = -dw/d\varphi_S$. On the right the black dot represents the director position as it rotates around the FLC's tilt cone, lying on the surface at $\varphi_S = 0$.

function $w(\varphi_S)$, the torque applied to the FLC by the surface at equilibrium is balanced by the elastic torque $Bd\varphi/dx$ applied to the surface by the FLC [Eq. (2b)]. As the applied voltage increases during switching, the dipole orientation at the surface will be driven further and further from its 0 V equilibrium position. Suppose that the maximum torque N_M applied by the surface occurs at φ_M and that the dipole is driven to that position at voltage V_{TF}. As the voltage increases beyond V_{TF} the dipole orientation advances beyond φ_M. At this point the opposing surface torque begins to decrease and can no longer balance the growing torque produced by the increasing voltage, so for $V > V_{TF}$ the FLC director jumps to the region of the other anchoring energy minimum, i.e., bistable switching occurs.

Here we want to investigate the dependence of threshold voltage V_{TF} on surface factors such as N_M and φ_M, on FLC parameters, and on the thicknesses of the FLC and alignment layers. The general procedure is to choose a set of values for φ_S, P_S, cell thickness, etc. (i.e., the FLC's orientation at the surfaces is pinned at a fixed value) and then to numerically compute the torque N applied to the surface by the FLC for a range of applied voltages V, producing a curve of V vs N. For a surface interaction energy $w(\varphi_S)$ whose maximum torque N_M occurs at $\varphi_M = \varphi_S$, the voltage V at which the torque applied to the surface equals N_M will be the threshold voltage V_{TF}. In the following sections families of curves are computed to explore how the threshold voltage varies with surface properties $\{\varphi_M, N_M\}$, FLC properties $\{P_S, B\}$, and cell parameters $\{L_F, L_A\}$. The numerically computed solutions are used together with approximate analytical solutions to identify key behaviors and their controlling factors.

III. $\varphi(x)$ SOLUTIONS: NUMERICAL AND ANALYTIC

To determine torques applied to the surfaces by the FLC we need to compute $Bd\varphi/dx$ and so need to know $\varphi(x)$. In this section we use numerical computations and approximate analytic expressions to gain insight into the behavior of $\varphi(x)$ solutions and their dependence on P_S, etc. Subsequent sections use these results to determine switching thresholds. We pay particular attention to the role of polarization stiffening and the related screening of applied drive voltage that occurs in the cell interior. Initially we consider only the voltage across the FLC layer; the influence of voltage drops across alignment layers is addressed starting in Sec. V.

A practical problem is how to choose a trial solution for the numerical differential equation solver (MATLAB was used for this work): The solver fails if the trial solution is too different from the actual solution. Here a two-step process was used. Rather than start with the Euler-Lagrange equations for static solutions we instead start with the time-dependent equations (not shown here) using a simple initial condition, e.g., $\varphi(x) = \varphi_S + 0.01\sin(\pi x/L_F)$. Once MATLAB's time-dependent numerical solver achieves an approximate steady-state solution it is used as the trial solution for the steady-state solver.

Figure 3(a) shows numerical solutions over a range of applied voltages for $\varphi_S = 45°$, $P_S = 25\,\mathrm{nC/cm^2}$, $B = 10\,\mathrm{pN}$, and a cell thickness of $L_F = 1.6\,\mu\mathrm{m}$. From 0 to 2.4 V the steps are in increments of 0.24 V. Equal steps in $(1/V)^{1/2}$ are used from 2.4 to 102 V. Solutions were obtained by numerically

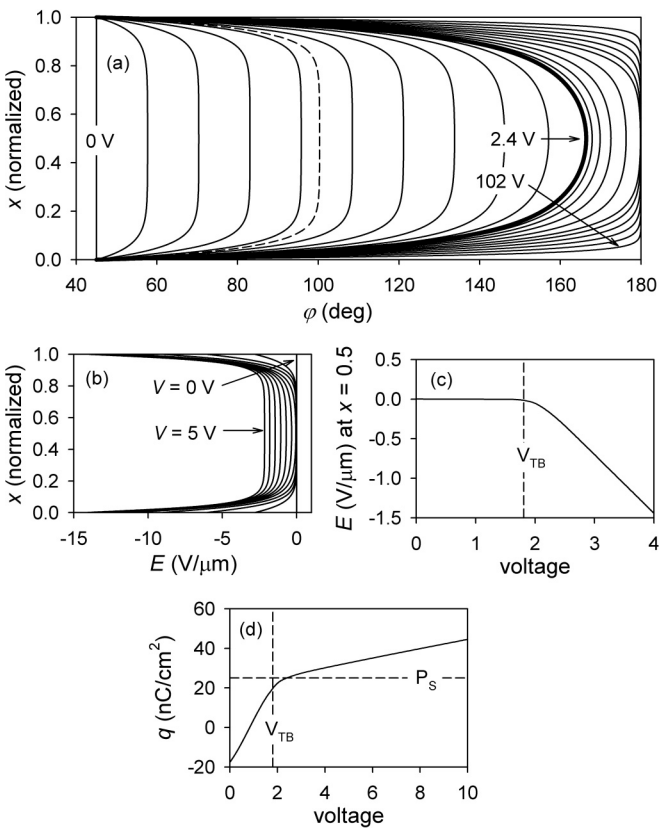

FIG. 3. The parameters are $L_F = 1.6\,\mu\mathrm{m}$, $L_A = 0$, $P_S = 25\,\mathrm{nC/cm^2}$, $B = 10\,\mathrm{pN}$, $\xi_P = 75\,\mathrm{nm}$, $\xi_P/L_F = 0.047$, $\varphi_S = 45°$, and $\varepsilon_F = 4\varepsilon_0$. (a) Plot of $\varphi(x)$ for voltages of 0–102 V. The heavy line is the $\varphi(x)$ corresponding to an applied charge of $q = P_S$, occurring at voltage $V_P = 2.4\,\mathrm{V}$. Below V_P the voltage is varied in steps of $0.1V_P$. Above, it varies from V_P to 102 V (where $q = 10P_S$) through ten equal steps in $(1/V)^{1/2}$. See the text regarding the dashed line. (b) Plot of the electric field strength $E(x)$ for $V = 0{-}5\,\mathrm{V}$ in steps of 0.5 V. (c) Plot of the midcell electric field strength ($x = 0.5L_F$) vs voltage. (d) Plot of q vs voltage.

solving Eq. (4) for a range of $\tilde{q}$ values, then using Eq. (5) to compute the corresponding voltages across the FLC layer (for $L_A = 0$), and then interpolating the family of $\varphi(x,V)$ curves to obtain $\varphi(x)$ curves at the desired voltages. For the fixed surface orientation φ_S these solutions can be used to compute the torque applied to the surface by the FLC ($N = Bd\varphi/dx$) vs voltage. The $V(N)$ curves computed by this procedure are used in later sections to compute threshold voltages.

Below about 2 V, $\varphi(x)$ is dominated by the characteristic length $\xi_P = 75\,\text{nm}\,(\xi_P/L_F = 0.05)$. In the central region of the cell ϕ is nearly constant and independent of x. Near surfaces ϕ varies approximately as $\exp(-x/\xi_P)$ (see Sec. III A) in order to satisfy the boundary condition $\varphi = \varphi_S$. At these low voltages the polarization charge screens the applied electric field, causing the electric field in the central portion of the cell to be nearly zero [Figs. 3(b) and 3(c)]. At low voltage we have in the center of the cell the simple relationship $P_S\cos\varphi \cong -q$, where $-q$ is the polarization charge needed to counterbalance charge q on the drive electrodes; this is a central concept of electrostatically controlled thresholdless switching [5–8]. Once $|q|$ approaches or exceeds P_S the FLC's polarization can no longer fully screen additional increases in the applied electric field; the internal field grows and the dominant characteristic length becomes $\xi_{PE}\,(<\xi_P)$, which shrinks with increasing voltage. The $\varphi(x)$ curve in Fig. 3(a) corresponding to the voltage at which $q = P_S$ is indicated by a thick line, where the voltage across the FLC layer is 2.4 V.

Figure 3(d) shows a plot of q vs V computed from $\varphi(x)$ curves that are numerical solutions of Eq. (4) [and using Eq. (5)]. At $V = 0$ the director field is uniform and the polarization surface charge $P_S\cos\varphi_S$ is exactly canceled by the surface charge $q = -P_S\cos\varphi_S$. As V grows from zero, the charge density q increases to pass through zero a little past the point where φ_{ctr} has become greater than 90° (dipole parallel to cell faces). Once V substantially exceeds ~2.4 V we have $\varphi(x) = 180^\circ$ and no more polarization charge is available to screen further increases in applied voltage.

A. Approximate analytic solutions

Although we lack an analytic solution to the nonlinear differential equation for $\varphi(x)$, the following ansatz serves as a useful empirical approximation for $2\xi/L_F \ll 1$ ($\xi \in \{\xi_P,\xi_{PE}\}$) and $\varphi_S \sim 45^\circ$:

$$\varphi = \varphi_{\text{ctr}} + 2(\varphi_S - \varphi_{\text{ctr}})e^{-L_F/2\xi}\cosh\left(\frac{x - L_F/2}{\xi}\right), \tag{7a}$$

$$|q|/P_S < 1: \quad \xi = \xi_P, \quad \cos\varphi_{\text{ctr}} = -\frac{q}{P_S}, \tag{7b}$$

$$|q|/P_S > 1: \quad \xi = \xi_{PE}, \quad \varphi_{\text{ctr}} = \pi. \tag{7c}$$

The dashed line in Fig. 3(a) is a $\varphi(x)$ curve computed for $V = 4 \times 0.24\,\text{V}$ using the above expressions and Eq. (5). This simple approximation produces curves that fall within about 10% of those obtained by numerical solution of the Euler-Lagrange equations, making the approximation useful for gaining insight into the principal physical mechanisms and dependencies.

Similarly, we make an ansatz that provides a useful approximation to the electric field $E(x)$ so long as $2\xi/L_F \ll 1$,

$$\begin{aligned} &E = E_{\text{ctr}} + 2(E_0 - E_{\text{ctr}})e^{-L_F/2\xi}\cosh\left(\frac{x - L_F/2}{\xi}\right),\\ &E_0 = -\varepsilon_F^{-1}(q + P_S\cos\varphi_S),\\ &|q|/P_S < 1: \quad \xi = \xi_P,\ E_{\text{ctr}} = 0,\\ &|q|/P_S > 1: \quad \xi = \xi_{PE},\ E_{\text{ctr}} = -\varepsilon_F^{-1}(q - P_S). \end{aligned} \tag{8}$$

The voltage across the FLC can be estimated by integrating the electric field [Eq. (8)]

$$|q|/P_S < 1: \quad V = 2V_B\left(\frac{q}{P_S} + \cos\varphi_S\right), \tag{9a}$$

$$|q|/P_S > 1: \quad V = \frac{(q - P_S)}{\varepsilon_F}L_F + 2V_B\sqrt{\frac{P_S}{|q|}}(1 + \cos\varphi_S), \tag{9b}$$

$$V_B = \sqrt{B/\varepsilon_F}. \tag{9c}$$

The slope of q vs V is the FLC layer's voltage-dependent capacitance $c_F = dq/dV$; approximate values for c_F can be obtained from Eq. (9). For $|q|/P_S < 1$ we have $c_F = \varepsilon_F/2\xi_P$, whereas $c_F = \varepsilon_F/[L_F - (P_S/q)\xi_{PE}(1 + \cos\varphi_S)]$ for $|q|/P_S > 1$, where ξ_{PE} shrinks with increasing q. As $|q|/P_S$ becomes very large the capacitance becomes simply $c_F = \varepsilon_F/L_F$. At small $|q|/P_S$ the capacitance is dominated by the thickness of the twist regions, whereas at large $|q|/P_S$ it is determined simply by the thickness of the FLC layer. For the example of Fig. 3(d) these approximations predict c_F values of 23 and 2.2 nF/cm^2, respectively, for the low- and high-$|q|/P_S$ limits, matching the curve of Fig. 3(d) to within 10%.

IV. THRESHOLD VOLTAGE CALCULATIONS

To compute the bistable switching threshold of the FLC layer alone (i.e., excluding alignment layers) for a given surface strength N_M (and φ_M), we compute curves of FLC voltage V vs the torque $N = (Bd\varphi/dx)|_{x=0}$ applied to the lower surface for a fixed surface dipole orientation of $\varphi_S = \varphi_M$. Torque at the $x = L_F$ surface is $-N$ in this symmetric geometry. The switching threshold V_{TF} is the voltage at which $(Bd\varphi/dx)|_{x=0} = N_M$. For the special case of Eq. (6) these curves are equivalent to plots of threshold voltage vs surface anchoring energy, i.e., $N_M = \gamma$.

Curves of V_{TF} vs N_M are computed by first numerically solving the Euler-Lagrange equation to obtain $\varphi(x)$ for a chosen value of q driven onto the cell's electrodes, with $\varphi_S = \varphi_M$ at both surfaces. The solution $\varphi(x)$ is then used to compute N and the corresponding voltage across the FLC.

Figure 4 shows computed curves of V_{TF} vs N_M used to identify qualitative dependences on φ_M, P_S, B, and FLC layer thickness L_F. Behaviors evident in these examples include the following: (i) There is a qualitative change in behavior above ~2 V, (ii) there is essentially no dependence on FLC thickness below ~2 V, (iii) the apparent critical voltage (~2 V) is independent of P_S, (iv) the critical voltage grows with increasing elastic constant B, and (v) threshold voltage drops slowly with N_M once below ~2 V.

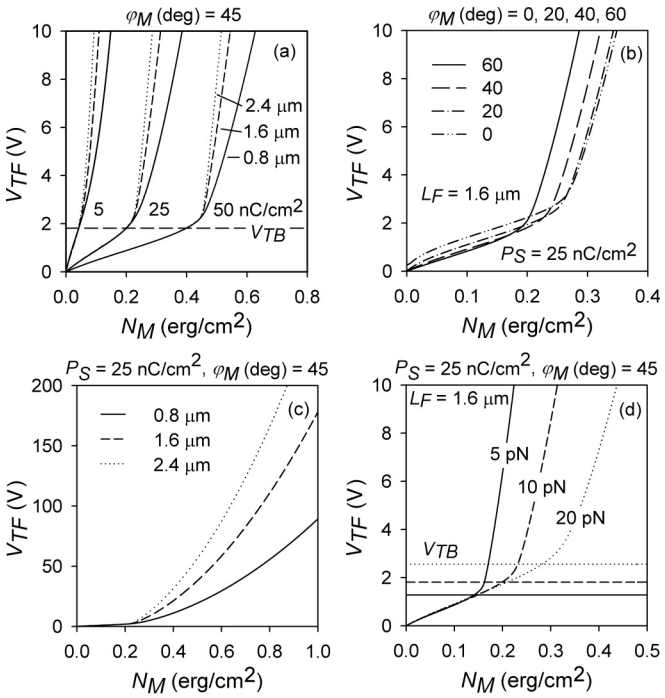

FIG. 4. Computed FLC threshold voltages V_{TF} vs surface torque density N_M, with $B = 10\,\text{pN}$ for (a)–(c): (a) three FLC layer thicknesses and three polarization values, (b) four peak torque angles φ_M, (c) a larger range of N_M at three thicknesses, and (d) three values of elastic constant B, where horizontal lines indicate corresponding values of V_{TB}.

Approximate expressions relating surface torque N to voltage V can be derived from Eqs. (7) and (9). From Eq. (7a) the torque applied to the surface by the FLC is found to be (for $\xi/L_F \ll 1, \xi \in \{\xi_P, \xi_{PE}\}$)

$$N = B\frac{d\varphi}{dx}\bigg|_{x=0} \cong B\frac{(\varphi_{\text{ctr}} - \varphi_M)}{\xi}. \tag{10}$$

The dependence of V on N is found by combining Eqs. (7), (9), and (10),

$$|q|/P_S < 1: \quad V = 2V_B\left[\cos\varphi_M - \cos\left(\varphi_M + \frac{N}{P_S V_B}\right)\right], \tag{11a}$$

$$|q|/P_S > 1: \quad V = \left\{\frac{P_S L_F}{\varepsilon_F}\left(\frac{N^2}{P_S^2 V_B^2(\pi - \varphi_M)^2} - 1\right) + \frac{2P_S V_B^2}{|N|}(\pi - \varphi_M)(1 + \cos\varphi_M)\right\}. \tag{11b}$$

A. The P_S-independent critical voltage V_{TB}

The critical voltage at which curves of V vs N change character can be estimated from Eq. (9). The voltage V_{TB} at which switching behavior crosses over from $|q|/P_S < 1$ to $|q|/P_S > 1$ is approximately the voltage at which Eqs. (9a) and (9b) become equal, which occurs at $|q/P_S| = 1$,

$$V_{TB} = 2V_B(1 + \cos\varphi_M) \cong 3.4\sqrt{B/\varepsilon_F}. \tag{12}$$

Here V_{TB} is P_S independent and the approximation applies for $\varphi_M = 45°$. For the example of Fig. 3 we have $V_{TB} = 1.8\,\text{V}$. The only dependence on FLC thickness and P_S is through the requirement that $2\xi_P/L_F \ll 1$ for the approximations to be valid (e.g., medium to high P_S in Table I). As is evident in Fig. 3(c), V_{TB} is the voltage above which the applied electric field can no longer be fully screened by the FLC's polarization. Consistent with behaviors (iii) and (iv) cited in the third paragraph of Sec. IV, the expression for V_{TB} depends only on B, ε_F, and the anchoring energy's φ_M.

B. Thickness independence of thresholds below V_{TB}

The voltage V_{TB} marks the transition between a director structure dominated by the characteristic length ξ_P to one dominated by ξ_{PE}. As is apparent in Fig. 4, the sensitivity of V_{TF} to changes in the surface's N_M and φ_M and to the FLC's P_S, B, and thickness L_F is very different for these two characteristic lengths (ξ_P and ξ_{PE}). Expressions for V_{TF} in the ranges $V_{TF} < V_{\text{TB}}$ and $V_{TF} > V_{\text{TB}}$ (i.e., $N/P_S V_B \ll 1$ and $N/P_S V_B \gg 1$) are found from Eq. (11),

$$V_{TF} \cong \frac{2N_M \sin\varphi_M}{P_S} \quad \text{for} \quad V_{TF} < V_{TB}, \tag{13a}$$

$$V_{TF} \cong \frac{L_F N_M^2}{B P_S(\pi - \varphi_M)^2} \quad \text{for} \quad V_{TF} > V_{TB}. \tag{13b}$$

For weak surfaces whose switching threshold is less than V_{TB} Eq. (13a) predicts that the threshold will be independent of FLC thickness, in agreement with numerical solutions shown in Fig. 4(a) and with behavior (ii) cited in the third paragraph of Sec. IV. Equation (13) also shows a linear dependence of V_{TF} on N_M below V_{TB} and a quadratic dependence above, matching the behavior of curves shown in Figs. 4(a) and 4(c).

For $V < V_{TB}$ the electric field in the interior of the FLC layer is essentially zero due to screening by polarization charge [Figs. 3(b) and 3(c)], thus the interior of the FLC layer makes no contribution to V regardless of its thickness. Voltage drops occur only across twist regions of thickness $\sim \xi_P$ near the surfaces. This is also why at low voltage the FLC capacitance depends only on ξ_P and not on L_F, as found in Sec. IV A.

In Eq. (11b) it appears that V could actually decrease with increasing FLC thickness for certain combinations of parameters. However, using $\varphi_{\text{ctr}} = \pi$ and $\xi = \xi_{PE}$ in Eq. (10) we find $q/P_S = N^2/[P_S{}^2 V_B{}^2(\pi - \phi_M)^2]$, thus the first line of Eq. (11b) becomes $(P_S L_F/\varepsilon_F)(q/P_S - 1)$. In the high-$q$ case of Eq. (11b) we of course have $q/P_S > 1$, so in fact V can only increase as the FLC thickness grows.

C. Barriers to reducing threshold voltage

In applications such as microdisplays [11], where the FLC is driven by low-voltage very large scale integrated (VLSI) circuitry, it is desirable to engineer the FLC cell to have the lowest possible switching threshold. Insight into how easy or how difficult it might be to reduce thresholds can be gained from studying the analytic solutions developed in preceding sections.

It seems intuitive that an FLC cell's threshold could be made arbitrarily small by increasing P_S, so we first examine the dependence of the threshold voltage on P_S for fixed surface

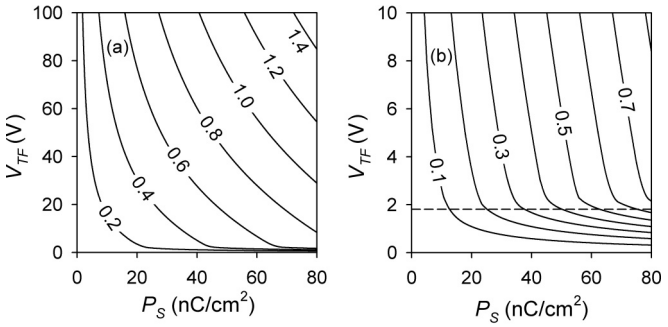

FIG. 5. (a) Numerically computed curves of V_{TF} vs P_S for surface strengths in the range $0.2-1.4\,\mathrm{erg/cm^2}$ for $L_A = 0$, $B = 10\,\mathrm{pN}$, $L_F = 1.6\,\mu\mathrm{m}$, $\varphi_M = 45^\circ$, and $\varepsilon = 4\varepsilon_0$. (b) Same as (a) but showing detail at low voltage and additional N_M curves; the dashed line marks V_{TB}.

strength N_M. Figure 5 shows $V_{TF}(P_S)$ curves for surface strengths in the range $0.2-1.4\,\mathrm{erg/cm^2}$ for the example of $L_A = 0$, $B = 10\,\mathrm{pN}$, $L_F = 1.6\,\mu\mathrm{m}$, $\varphi_M = 45^\circ$, and $\varepsilon = 4\varepsilon_0$. A set of V_{TF} vs N_M curves was computed numerically for a range of P_S values just as was done for Fig. 4. The $V_{TF}(P_S)$ curves were obtained by interpolation of the computed (V_{TF}, N_M, P_S) data set.

It is clear from Fig. 5 that there is a large change in the threshold's sensitivity to changes in P_S as the threshold passes through V_{TB}. This change in sensitivity can by studied by using Eq. (13) to obtain and compare estimates of dV/dP_S for thresholds above and below V_{TB},

$$\frac{(dV_{TF}/dP_S)|_{V_{TF}>V_{TB}}}{(dV_{TF}/dP_S)|_{V_{TF}<V_{TB}}} \cong \frac{L_F N_M}{2B(\pi-\varphi_M)^2\sin\varphi_M} = \frac{N_M}{7.8B/L_F} \quad \text{for} \quad \varphi_M = \frac{\pi}{4}. \tag{14}$$

For the representative values $B = 10\,\mathrm{pN}$ and $L_F = 1.6\,\mu\mathrm{m}$ we have $B/L_F = 6.25\times10^{-6}\,\mathrm{J/m^2}$ $(6.25\times10^{-3}\,\mathrm{erg/cm^2})$. At a surface strength of $N = 0.5\,\mathrm{erg/cm^2}$ [a contour in Fig. 5(b)] the threshold voltage becomes 10 times less sensitive to further increases in P_S as it passes below V_{TB}, consistent with the sharp change of slope seen in Fig. 5.

Insight into the cause of the threshold voltage's change in sensitivity to P_S at V_{TB} can be gained by examining Fig. 3(a) and Eq. (10). Torque applied to the surface grows as $dN = (B/\xi)d\varphi_{\mathrm{ctr}} - (B\varphi_{\mathrm{ctr}}/\xi^2)d\xi$. At low voltage $(V < V_{TB})$ the dominant characteristic length ξ_P is voltage independent and torque applied to the surface by the FLC [i.e., $(Bd\varphi/dx)|_{x=0}$] grows only due to changes in φ_{ctr} (e.g., $\cos\varphi_{\mathrm{ctr}} = -q/P_S$). At higher voltage $(V > V_{TB})$ φ_{ctr} continues to grow and the dominant characteristic length becomes ξ_{PE}. Further, ξ_{PE} shrinks with further increases in voltage so both $d\varphi_{\mathrm{ctr}}$ and $d\xi$ contribute to increasing torque.

Another approach to reducing the threshold voltage is of course to develop FLC and alignment surface combinations having weaker surface interactions N_M. It is apparent from Fig. 4 that reducing surface strength has a large effect in lowering the threshold for voltages above V_{TB}, but it is much less effective in further lowering the voltage once below. Using Eq. (13) again, we can obtain and compare estimates of dV_{TF}/dN_M for thresholds above and below V_{TB},

$$\frac{(dV_{TF}/dN_M)|_{V_{TF}>V_{TB}}}{(dV_{TF}/dN_M)|_{V_{TF}<V_{TB}}} \cong \frac{L_F}{\xi_P}\frac{1}{(\pi-\varphi_M)\sin\varphi_M} = \frac{L_F}{1.6\xi_P} = \frac{L_F P_S}{1.6\sqrt{\varepsilon_F B}} \quad \text{for} \quad \varphi_M = \frac{\pi}{4}. \tag{15}$$

For the representative values of $B = 10\,\mathrm{pN}$, $L_F = 1.6\,\mu\mathrm{m}$, $P_S = 25\,\mathrm{nC/cm^2}$, and $\varepsilon = 4\varepsilon_0$ [Fig. 4(a)] we have $\xi_P = 75\,\mathrm{nm}$. With $\varphi_M = \pi/4$, V_{TF} is 13 times less sensitive to changes in N_M when below V_{TB} than when above, accounting for the sharp change of slopes seen in Fig. 4.

The above analysis shows that the bistable switching threshold becomes an order of magnitude less sensitive to decreases in FLC polarization and surface strength once V_{TF} has been reduced to below V_{TB}, which explains behaviors (i) and (v) identified in the third paragraph of Sec. IV. This implies that it may be difficult to engineer bistable FLC layers having thresholds much below V_{TB}.

V. COMPLETE CELL WITH ALIGNMENT LAYERS

Dielectric alignment layers can substantially alter an FLC cell's switching behavior, thick alignment layers can induce an otherwise bistable FLC cell to exhibit thresholdless switching [7], and even thin alignment layers can reduce how fully a bistable FLC cell can switch [6]. The approximate analytical solutions devised in the preceding sections can be used to investigate (a) whether alignment layers increase or decrease the switching threshold, (b) the minimum surface strength needed to maintain bistability as alignment layer thickness L_A increases, and (c) the transition from bistable to analog (thresholdless) switching.

A. Threshold vs L_A

When a charge q is driven onto an FLC cell the resultant voltage V_{cell} is given by Eq. (16a), where V_F is the voltage across the FLC layer. Expressions for q in the high- and low-$|q|/P_S$ limits (i.e., $V_F > V_{TB}$ and $V_F < V_{TB}$) can be obtained from Eqs. (9a) and (9b), respectively; inserting these expressions for q into Eq. (16a) yields expressions showing the influence of alignment layer thickness on the cell's threshold voltage $V_{T\mathrm{cell}}$. These relationships are valid for $2\xi_P/L_F \ll 1$ (e.g., medium to high P_S in Table I):

$$V_{\mathrm{cell}} = V_F + \frac{2L_A q}{\varepsilon_A}, \tag{16a}$$

$$V_{TF} < V_{TB}: \quad V_{T\mathrm{cell}} = V_{TF} + \left(\frac{V_{TF}}{2V_B} - \cos\varphi_M\right)\frac{2L_A P_S}{\varepsilon_A}, \tag{16b}$$

$$V_{TF} > V_{TB}: \quad V_{T\mathrm{cell}} = V_{TF} + \left(1 + \frac{\varepsilon_F V_{TF}}{P_S L_F}\right)\frac{2L_A P_S}{\varepsilon_A}. \tag{16c}$$

For $V_{TF} > V_{TB}$ the cell threshold V_{Tcell} increases with growing alignment layer thickness just as might be expected. However, for $V_{TF} < V_{TB}$ the presence of the alignment layer

can either raise *or* lower the cell's threshold voltage depending on whether $V_{TF}/2V_B\cos\varphi_M$ is greater than or less than 1.

From Eq. (16a) we see that $V_{\rm cell}$ decreases with increasing alignment layer thickness when $q < 0$. In the example of Fig. 3(d) $q < 0$ occurs for $\varphi_{\rm ctr} <\sim 90^\circ$, where $|q|/P_S < 1$ and $V < V_{TB}$. So, consistent with Eq. (16b), the presence of the alignment layer can reduce the cell's bistable switching threshold when V_{TF} is less than V_{TB}. However, in this case, electro-optic bistability would be poor due to the small range of optic axis rotation (Sec. V C).

B. Minimum surface strength for bistability (backswitching limit)

An FLC cell can be considered to be bistable if the state it is switched to by a positive or negative voltage pulse is maintained indefinitely after the cell voltage is returned to zero. If an FLC cell is fully switched there will be a charge of P_S present at the surface of the FLC layer; the alignment layer must have a compensating negative charge to make the total cell voltage zero. As a consequence, with 0 V applied to the FLC cell there will be a voltage of magnitude $P_S/(\frac{1}{2}c_A + c_F)$ across the FLC layer that drives the FLC away from being fully switched (c_F and c_A are the FLC and alignment layer capacitances per unit area). The FLC switching threshold V_{TF} must be high enough to resist this backswitching [12] voltage. Of course backswitching can be completely eliminated by using conductive rather than dielectric alignment layers [13].

Since we are looking for the minimum surface strength needed to maintain bistability we need consider only the case $\xi_P < \xi_{PE}$ (i.e., $|q|/P_S < 1$). The voltage present on the FLC layer when the cell voltage is zero can be determined by first finding the value of q required to make $V_{\rm cell} = 0$ [using Eqs. (16a) and (9a)] and then inserting the expression for q into Eq. (9a) to determine the FLC voltage V_F,

$$V_F(V_{\rm cell} = 0) = 2V_B\left(1 + \frac{\varepsilon_A}{\varepsilon_F}\frac{\xi_P}{L_A}\right)^{-1}\cos\varphi_M. \qquad (17)$$

The FLC switching threshold must be greater than this value to ensure bistability. As L_A becomes large ($L_A \gg \xi_P$), the FLC layer threshold voltage V_{TF} must be greater than $2V_B\cos\varphi_M$ in order to ensure bistability ($\sim$0.75 V for $B =$ 10 pN, $\varepsilon_F = 4\varepsilon_0$, and $\varphi_M = 45^\circ$). For thin alignment layers the minimum required threshold voltage is approximately $(\varepsilon_F/\varepsilon_A)(L_A/\xi_P)\cos\varphi_M$, which is proportional to P_S and goes to zero along with L_A. In the above example, the minimum FLC layer threshold voltage needed to ensure bistability with 20 nm alignment layers is $\sim$0.2 V ($\varepsilon_F = \varepsilon_A = 4\varepsilon_0$, $B =$ 10 pN, $P_S = 25\,{\rm nC/cm^2}$, and $\varphi_M = 45^\circ$).

The corresponding minimum surface strength N_M needed to ensure bistability can be determined by comparing Eq. (17) to Eq. (11a). The condition for bistability is

$$\cos\left(\varphi_M + \frac{N_M}{P_S V_B}\right) < \left(1 + \frac{\varepsilon_F}{\varepsilon_A}\frac{L_A}{\xi_P}\right)^{-1}\cos\varphi_M \qquad (18)$$

In the limit as the alignment layer becomes very thick ($L_A \gg \xi_P$) this requires $N_M > P_S V_B(\pi/2 - \varphi_M)$. In the limit as the alignment layer thickness approaches zero this requires $N_M > (L_A {P_S}^2/\varepsilon_A)\cot\varphi_M$ [or $(\varepsilon_F/\varepsilon_A)(L_A/\xi_P)P_S V_B\cot\varphi_M$]. For $B =$ 10 pN, $P_S = 25\,{\rm nC/cm^2}$, $\varepsilon_F = 4\varepsilon_0$, and $\varphi_M = 45^\circ$, the minimum surface strength needed to maintain bistability in the presence of thick alignment layers is 0.1 erg/cm^2. For a thin 20 nm alignment layer the minimum surface strength is 0.035 erg/cm^2. If typical FLC cell surfaces have strengths on the order of [10] 1 erg/cm^2, then low- to medium-P_S FLC cells should in general be bistable.

C. Transition between thresholdless and bistable switching

Opposite to the extreme of pure bistability is thresholdless switching (also known as V shaped), in which dipole orientation φ obeys the simple relationship $V = -(2L_A P_S/\varepsilon_A)\cos\varphi$, where φ is uniform throughout the cell [5,6] [e.g., set $Q/A = -P_S\cos\varphi$ in Eq. (5)]. It has been shown that thresholdless behavior is expected in FLC cells having high P_S and thick alignment layers or with thin alignment layers and charge control drive [7,14] where a large bulk electrostatic energy overwhelms surface forces to induce thresholdless behavior [7] ($4\gamma\varepsilon_F/L_F P_S^2 < 1$). In those extreme cases the strength and φ_S dependence of the surface interaction energy become unimportant.

When considering the FLC cell as a bistable optical switch we would like $\varphi_{\rm ctr}$ to be as close to zero as possible at $V_{\rm cell} =$ 0 in order to maximize optic axis rotation from one stable state to the other. At $V_{\rm cell} = 0$ V we have from combining Eqs. (7b), (9a), and (16b) (for low-threshold switching $V_{TF} < V_{TB}$)

$$\cos\varphi_{\rm ctr} = \left(1 + \frac{P_S L_A}{\varepsilon_A V_B}\right)^{-1}\cos\varphi_M. \qquad (19)$$

Here $\varphi_{\rm ctr}$ can be no smaller than φ_M, so surface energy functions having a narrower minimum than in the example of Fig. 2 are preferred (to bring φ_M closer to zero). Further, in order for $\varphi_{\rm ctr}$ to be as small as possible, we also want

$$L_A \ll \xi_P\frac{\varepsilon_A}{\varepsilon_F}, \qquad (20)$$

where we have used $\xi_P = (\varepsilon_F B)^{1/2}/P_S$ in Eq. (19). The alignment layer must be thinner than a twist region in order to achieve good bistability; this is complementary to the condition $L_A \gg \xi_P$ found to be required for voltage-driven thresholdless switching [7] (in contrast to charge drive with $L_A \sim 0$).

The results of previous sections can also be used to investigate situations intermediate to the extremes of bistable and thresholdless behavior. Starting with a high-threshold case and strong surface where $V_{TF} > V_{TB}$ [Eq. (16c)] we can approach a zero threshold for the cell by reducing both V_{TF} (e.g., reducing surface strength) and L_A. However, it seems unrealistic that V_{TF} could actually be reduced to zero and as V_{TF} becomes smaller we eventually pass to the case of $V_{TF} < V_{TB}$ and must switch to using the voltage threshold expression of Eq. (16b).

It is apparent in Eq. (16b) that increasing the alignment layer thickness can reduce a cell's threshold to zero for nonzero V_{TF} if the term in parentheses is negative, i.e., $V_{TF} < 2V_B\cos\varphi_M$. For the example $\varepsilon_F = \varepsilon_A = 4\varepsilon_0$, $B =$ 10 pN, $P_S = 25\,{\rm nC/cm^2}$, and $\varphi_M = 45^\circ$, this means we must have $V_{TF} < 0.75$ V ($N_M < 0.13\,{\rm erg/cm^2}$ for $L_F =$ 1.6 μm [Fig. 4(d)]). If FLC polarization is raised to around

200 nC/cm^2 then a zero cell threshold can be achieved for surfaces as strong as ~1 erg/cm^2 (perhaps typical of polymer alignment surfaces [10]). At $N_M = 1$ erg/cm^2 and $P_S = 300$ nC/cm^2 an alignment layer thickness of only 20 nm would be sufficient to achieve $V_{Tcell} = 0$. However, $\cos\varphi_{\rm ctr}/\cos\varphi_M = 0.24$ [Eq. (19)], so electro-optic bistable switching would become poor as this limit is approached, i.e., the memory angle (Sec. VII) becomes small and the cell approaches thresholdless behavior.

VI. CHEVRONS PLUS ALIGNMENT LAYERS

To accommodate chevrons we must include layer tilt and must add an energy term that characterizes the chevron interface (where layers of differing tilt meet). The chevron interface is introduced by adding a surface energy term to the free energy [15] (here differing slightly from the cited reference)

$$\begin{aligned} w_{\rm ch}(\varphi_L,\varphi_U,\delta_L,\delta_U,\theta_T) &= -\gamma(\hat{\mathbf{n}}_L\cdot\hat{\mathbf{n}}_U)^2, \\ \hat{\mathbf{n}}_L\cdot\hat{\mathbf{n}}_U &= \cos^2\theta_T\cos(\delta_L-\delta_U)+[\cos\varphi_L\cos\varphi_U \\ &\quad +\sin\varphi_L\sin\varphi_U\cos(\delta_L-\delta_U)]\sin^2\theta_T \\ &\quad +\frac{1}{2}(\sin\varphi_U-\sin\varphi_L)\sin 2\theta_T\sin(\delta_L-\delta_U), \end{aligned} \tag{21}$$

where subscripts L and U refer, respectively, to values of φ and layer tilt angle δ (Fig. 6) immediately below and above the chevron discontinuity and θ_T is the FLC tilt angle (Fig. 1).

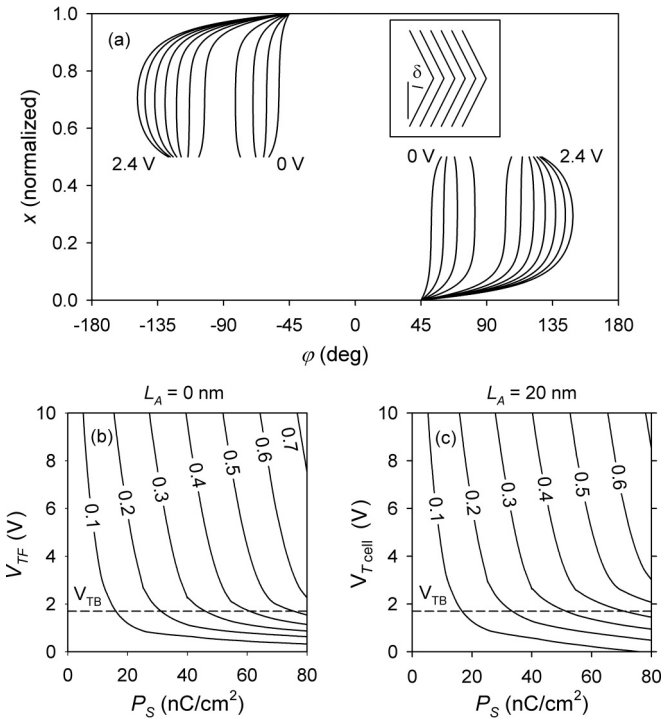

FIG. 6. (a) The $\varphi(x)$ solutions for 11 FLC voltages ranging from 0 to 2.4 V in steps of 0.24 V. The inset illustrates the definition of the chevron angle δ. See the text for FLC and cell parameters. (b) Computed curves of V_{TF} vs P_S for surface strengths N_M in the range 0.1−0.7 erg/cm^2. (c) Same as (b), except plotting V_{Tcell} vs P_S for 20 nm alignment layers ($\varepsilon_A = 4\varepsilon_0$).

Director orientations at the chevron interface are represented by $\hat{\mathbf{n}}_L$ and $\hat{\mathbf{n}}_U$, and $w_{\rm ch}$ has two minima at which the upper and lower directors are parallel to each other and to the planar chevron interface at $x = L_F/2$.

From inspection of Eq. (1) it is apparent that tilting the smectic layers by an angle δ has the effect of rescaling the space derivative and the x component of the polarization

$$\frac{d^2\varphi}{dx^2}\to\cos^2\delta\frac{d^2\varphi}{dx^2},\quad \mathbf{P}\cdot\hat{\mathbf{x}}\to P_S\cos\delta\cos\varphi. \tag{22}$$

In the symmetric chevron case considered here δ changes sign at $x = L_F/2 : \delta_L = -\delta_U = \delta$. These substitutions leave the Euler-Lagrange equation (2) unchanged except for a redefinition of the characteristic length ξ_{PE} (ξ_P is unchanged):

$$\xi_{PE} = \sqrt{\frac{B\cos\delta}{P_S|E_Q|}}. \tag{23}$$

Adding layer tilt in effect replaces B by $B\cos^2\delta$ and P_S by $P_S\cos\delta$. The expression for V_{TB} becomes

$$V_{TB} = 2\cos\delta\sqrt{B/\varepsilon_F}(1+\cos\varphi_M). \tag{24}$$

At $\delta = 20^\circ$ the voltage V_{TB} shrinks by only 6% and ξ_{PE} by only 3%. In the absence of other influences the presence of the chevron might be expected to slightly lower the voltage at which the knee in the curves of V_{TF} vs P_S, etc., occur. However, the form and strength of the chevron energy term (21) can have a large influence on $\varphi(x)$ and therefore potentially also on V_{TB}.

Figure 6(a) shows numerically computed solutions for $\varphi(x)$ at a chevron strength of $\gamma = 1$ erg/cm^2, $\delta = 20^\circ$, and $\theta_T = 22^\circ$; other parameters are the same as in Fig. 5. Here we have assumed a high pretilt surface (e.g., obliquely deposited SiO_2) for which the pretilt angle is equal to the chevron angle. Unlike in Fig. 5, dipoles in the upper and lower halves of the cell rotate in opposite directions in response to the applied voltage. Inspection of the voltage dependence of $\varphi(x)$ curves in Fig. 6(a) at $x = 0.5$ indicates that, in this example, chevron switching occurs at about 0.8 V.

Figure 6(b) shows curves of V_{TF} vs P_S for a range of surface strengths N_M. Compared to Fig. 5 (no chevron), slightly higher voltage or polarization is needed to achieve the same surface torque.

Figure 6(c) shows curves of V_{Tcell} vs P_S after including the effect of 20 nm alignment layers. Compared to Fig. 6(b), curves for weak surfaces (e.g., 0.1 erg/cm^2) shift to lower voltage while curves for stronger surfaces (e.g., 0.6 erg/cm^2) shift to higher voltage, in qualitative agreement with Eq. (16).

VII. EXAMPLE: HIGH PRETILT CELLS

Ferroelectric liquid crystal cells using obliquely deposited SiO_2 alignment layers are good examples of low-voltage bistable switching [16–18]. Thresholds exhibited by these cells are among the lowest of the dozens of FLCs and many alignment layers tested at Displaytech where this work was performed. They are therefore good candidates for testing expectations set by the model: to check the dependence of threshold voltage on FLC layer thickness and to compare the cell's measured threshold voltage to V_{TB}, which is expected to

be a practical lower limit below which it is difficult to further lower a cell's threshold (Sec. IV C).

For this investigation cells were made of indium tin oxide–coated glass substrates onto which SiO_2 was deposited at a near-grazing incidence angle of 5°, with a thickness of approximately 25 nm. Cells were assembled so that the deposition directions of opposing substrates were parallel. The cells were filled with the FLC Felix-019-100 from Clariant, having $P_S = 39\,\mathrm{nC/cm^2}$ at 25 °C, with estimated values of $B = 10\,\mathrm{pN}$ and $\varepsilon_F = 4$ for the FLC's elastic and dielectric constants.

Felix-019-100 aligns well on SiO_X [16], but not as well on the oblique SiO_2 used here, although certain Displaytech FLCs do [17,18]. Nevertheless, the small domains of aligned Felix-019-100 within the cells used here were large enough for switching studies, i.e., large enough to fill the field of view of a microscope. The better aligning Displaytech FLCs were not used here because of their proprietary nature (they are not generally available).

From the FLC's properties we compute $\xi_P = 0.05\,\mu\mathrm{m}$, which is more than a factor of 10 smaller than the smallest of the FLC gap thicknesses used here (0.8 and 2.4 μm), and $V_{TB} = 1.8\,\mathrm{V}$. The portion of the cell's switching threshold expected to arise from factors other than the FLC layer's threshold can be computed from Eq. (16b) or (16c) depending on whether V_{TF}/V_{TB} is greater or less than 1, obtaining values of $(V_{T\mathrm{cell}} - V_{TF}) = 0.44$ and $0.65\,\mathrm{V}$, respectively, for $L_F = 0.8\,\mu\mathrm{m}$. We of course do not know the value of V_{TF}, but the model suggests that it would most likely be comparable to or greater than V_{TB}, implying a cell threshold of $V_{T\mathrm{cell}} \sim 2.3\,\mathrm{V}$.

As stated in Sec. V C, an FLC cell can be considered to be bistable if the state it is switched to by a positive or negative voltage pulse is maintained indefinitely after the cell voltage is returned to zero. The pulse widths must of course be long enough for the FLC to switch before the voltage is returned to zero and the duration of the 0 V time must similarly be long enough for the FLC to settle. In these tests a pulse width is chosen and then its amplitude is varied while measuring the FLC cell's optic axis position during the 0 V time between pulses. The bistable switching threshold is the minimum pulse amplitude that leaves the FLC optic axis fully switched at 0 V. Due to details of the FLC cell's switching dynamics [19–21] (beyond the scope of this investigation) the apparent threshold drops toward an asymptotic value as the pulse width increases. By making measurements over a wide enough range of pulse widths we can extrapolate to the FLC cell's apparent quasistatic (infinite pulse width) response in order to allow comparison with the model.

The measurement system was fully automated. Drive voltage waveforms were computer controlled and systematically varied and a computer-driven rotation stage together with a polarizing microscope and photodetector was used to determine the FLC cell's optic axis position. As a check, FLC cells were also observed visually through a polarizing microscope while manually raising and lowering the cell voltage; bistable switching was evident both from the transient appearance of up and down domains and from measurement of the fully switched optic axis positions. It was found that threshold voltages obtained from the systematic automated measurements correlated well with the less precise threshold voltages that could be inferred from these manual, visual observations of bistable switching.

Cells were driven with a bipolar pulse waveform having a period of 24 ms, with drive set to 0 V between pulses. Pulse widths ranging from 0.25 to 8 ms were used and for each width the pulse amplitude was varied in steps of 0.1 V while measuring the FLC optic axis orientation during the last 2 ms of each 12 ms half period (i.e., with 0 V applied, immediately prior to the subsequent pulse). The memory angle is defined to be the difference between measured optic axis positions following sequential positive and negative pulses. Measured curves of memory angle vs pulse voltage are shown in Fig. 7(a) for the 0.8 μm cell, at pulse widths indicated by the data points of Fig. 7(b). Memory angle data for the 2.4 μm cell were similar.

A memory angle of zero indicates that the FLC optic axis (averaged across the field of view of the microscope) was unchanged by the voltage pulse. In this subthreshold condition the FLC within the microscope's field of view may be a single uniform domain or a mix of up and down domains. In fully switched states (memory angle of 42°) the FLC within the microscope's field of view is a single uniform up or down domain.

Threshold voltages were estimated by passing smooth curves through the memory angle data points of Fig. 7(a) and then using those curves to interpolate the voltage at which the memory angle had risen to 50% of its fully switched value of 42°. Measured values of threshold voltage vs pulse width for the two cells are shown in Fig. 7(b). The computed value

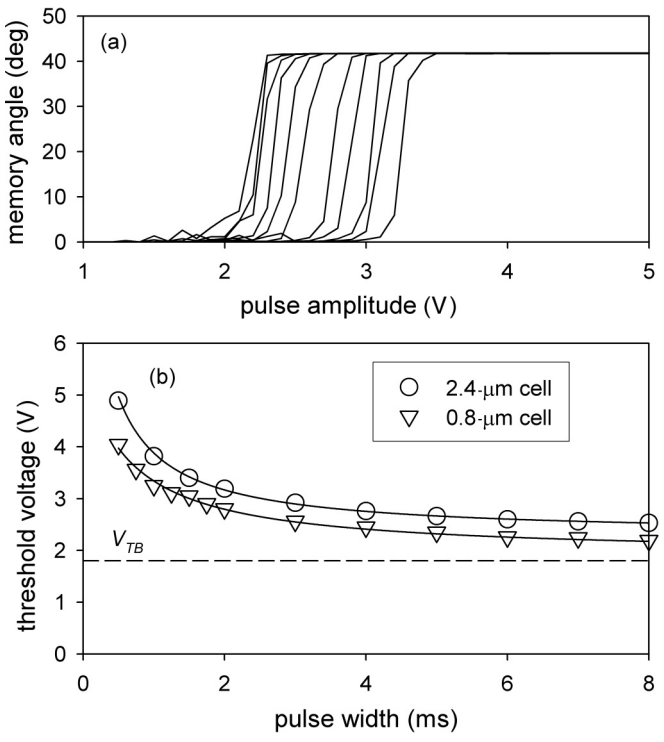

FIG. 7. (a) Measured curves of memory angle vs pulse amplitude for the pulse widths shown in (b). Switching at lower voltage corresponds to a greater pulse width. (b) Measured threshold voltage vs pulse width for two cell thicknesses.

of $V_{TB} = 1.8$ V (Sec. IV A) is indicated by a dashed line for reference.

The threshold data of Fig. 7(b) were fit by an empirically chosen curve of the form $V_T = V_\infty + A/\tau_P$, where τ_P is the pulse width; the fitted curves are shown as lines passing through the data points of Fig. 7(b). The V_∞ values for the 2.4 and 0.8 μm cells were 2.3 and 1.9 V, respectively, close to the computed estimate of $V_{T\text{cell}} \sim 2.3$ V. Although one cell is 3 times thicker than the other, its threshold voltage is only 20% larger, consistent with the model.

Excessive charge flow from ionic impurities within an FLC can degrade or destroy bistability [22,23]. The well-behaved bistable switching observed here and in similar cells [18] implies that in this case any ionic charge flow was too small to have a significant deleterious effect. Also, measurements of electrical current during the drive cycle showed little charge flow beyond the $\sim 2P_S$ expected for bistable switching. So, although we have no detailed knowledge of ion densities, mobilities, or their dynamics during bistable switching, we can infer that their effects were not large enough to seriously interfere with bistable switching over the range of voltages and time intervals used in these tests. It is also worthwhile to note that these cells exhibit long-term bistability, i.e., open-circuit cells left for days or weeks remained in their switched state. The apparent lack of any strong effects from ionic charge flow supports the validity of applying the ion-free static model developed in preceding sections.

VIII. FREDERIKS-LIKE THRESHOLD

Numerical solutions of V_{TF} vs N_M [Fig. 4(b)] for nonzero φ_M appear to pass through the origin (0,0), but as φ_M approaches zero (**P** perpendicular to cell surfaces) the curve jumps to $V_{TF} > 0$ at $N_M = 0$. This corresponds to a Frederiks threshold that has been studied in elastic-hydrodynamic modeling of SSFLC switching dynamics by Carlsson *et al.* [24]. In that study a critical field strength is found for the threshold; multiplying by the thickness of the FLC layer yields an expression for the Frederiks transition threshold voltage

$$V_{\text{Fred}} \equiv \frac{\pi^2 B}{P_S L_F}. \tag{25}$$

As the voltage is raised from zero (starting with $\varphi_S = 0$, **P** perpendicular to cell surfaces), torque applied to the surface remains at zero until the applied voltage exceeds V_{Fred}. For the case illustrated in Fig. 4(b) (and Fig. 8) we have $V_{\text{Fred}} = 0.25$ V, in good agreement with the numerical solutions.

IX. SUMMARY AND DISCUSSION

Bistable FLCs have been investigated for possible use in microdisplays, exhibiting switching thresholds low enough for CMOS VLSI drive [17,18,25]. The work reported here began as an effort to understand what fundamental limits there might be to lowering the voltage threshold of bistable FLC cells and to understand why it seemed difficult in practice to develop cells having thresholds below about 2 V.

As a starting point, a commonly used model for director structures within bookshelf smectic layer FLC's was used, incorporating elements thought to be essential while omitting

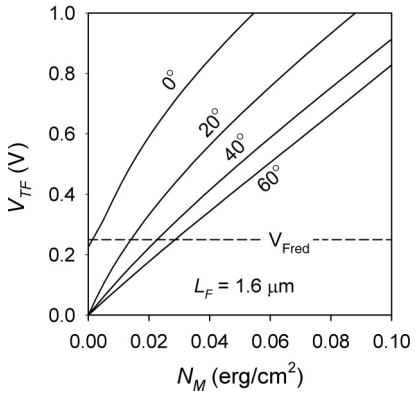

FIG. 8. Same as Fig. 4(b) but with expanded scales to show detail at low voltage, for $\varphi_M = 0°$, 20°, 40°, and 60°.

factors that seemed likely to add unnecessary complexity for the purpose of this investigation (e.g., dielectric anisotropy, ionic conductivity, and dynamics). Real FLC cells typically have chevron [1] smectic layers rather than bookshelf; the possible effects of this added complexity were addressed in Sec. VI. A simple form of surface interaction energy was used here that is expected to be at least qualitatively representative of real bistable FLC cells. The results obtained here are more general, however, and not dependent upon the specific form of the surface interaction.

Despite simplifications, analytic solutions are difficult to obtain for this nonlinear system. Here a hybrid approach of numerical techniques plus an ansatz of approximate analytical solutions was devised to overcome this difficulty. It was found that the polarization stiffening length ξ_P, perhaps best known for its role in thresholdless switching, in fact also plays a key role in bistable switching. Table I uses the ratio of ξ_P to alignment and FLC layer thickness to divide FLC cells into three categories expected to have qualitatively different behaviors, ranging from bistable (low- to medium-P_S) to thresholdless (e.g., high-P_S, thick alignment layers) switching. So long as the polarization stiffening length ξ_P is small compared to the thickness of the FLC layer, its ratio to alignment layer thickness ξ_P/L_A was found to control whether bistable ($L_A < \xi_P$) or thresholdless ($L_A > \xi_P$) switching is obtained (Sec. V). It has been shown elsewhere [7,14] that thresholdless switching can be obtained even with thin alignment layers ($\xi_P/L_A > 1$) if charge drive instead of voltage drive is used.

As the voltage on the FLC layer is raised, bistable switching occurs when the magnitude of the torque applied to the surface by the FLC ($B|d\varphi/dx|_S$) exceeds the maximum opposing torque that can be exerted by the surface on the FLC (Sec. II). For fixed voltage the surface torque $B|d\varphi/dx|_S$ grows with increasing polarization P_S. Further, $|d\varphi/dx|_S$ grows relatively rapidly with increasing P_S starting at low polarization and then grows much more slowly once $\xi_P = (\varepsilon_F B)^{1/2}/P_S$ becomes less than the thickness of the FLC layer, the transition occurring at an applied charge density of $|q| \cong P_S$ and FLC layer voltage of $V_{TB} \cong 3.4(B/\varepsilon_F)^{1/2}$ (Sec. IV A) that is independent of P_S. Two important consequences follow from this. First is that the FLC cell's threshold voltage becomes largely independent of FLC layer thickness once $\xi_P \ll L_F$. Essentially the entire FLC layer voltage drops across the twist layers of thickness

$\sim \xi_P$, leaving the electric field within the interior of the cell to be ~0 and making the FLC layer voltage independent of its thickness. Second, once an FLC layer threshold of $\sim V_{TB}$ has been reached, it becomes difficult to further lower the cell's threshold voltage by further weakening the surface or raising P_S (Sec. IV) and without reducing memory angle (Sec. V). This may explain why, in practice, it has been difficult to develop bistable FLC cells having thresholds below ~2 V.

As an experimental test of the model a combination of FLC and alignment surface was chosen as representative of low-threshold FLC cells; examples were fabricated in which the FLC layer thicknesses differed by a factor of 3. Despite the 3× difference in FLC layer thickness, the thresholds of these cells differed by only about 20% and the measured threshold voltages of 1.8–2.3 V were a good match to the model's prediction of ~2.3 V.

The model developed here provides a framework for understanding and further developing the design of bistable FLCs and cell surfaces, as well as explaining how FLC cells transition from bistable to thresholdless as parameters are changed. A remaining challenge for bistable FLC cells is that the range of drive conditions and temperature over which good alignment is maintained [26,27] must be expanded in order to be ready for commercial use. Also, this investigation has focused on the static or quasistatic bistable switching characteristics of FLC cells; a more complete understanding may require the inclusion of dynamics such as the formation and propagation of up and down domain walls [28], viscosities and flow [24,29,30], and ionic conductivity of the FLC layer due to impurities [22,23,31–34]. In addition, because its effects grow as E^2, dielectric anisotropy [omitted in Eq. (1)] may play an important role in the thin twist regions of some FLCs, affecting both length scales and surface torques.

ACKNOWLEDGMENTS

The author thanks Su Yang for assistance with cell preparation and threshold measurements and Joe Maclennan for valuable comments on a draft version of this manuscript.

[1] S. T. Lagerwall, *Ferroelectric and Antiferroelectric Liquid Crystals* (Wiley-VCH, Weinheim, 1999).
[2] A. Hammarquist, K. D'Havé, M. Matuszczyk, N. A. Clark, J. E. Maclennan, and P. Rudquist, Phys. Rev. E **77**, 031707 (2008).
[3] S. Inui, N. Iimura, T. Suzuki, H. Iwane, K. Miyachi, Y. Takanishi, and A. Fukuda, J. Mater. Chem. **6**, 671 (1996).
[4] T. Yoshida, T. Tanaka, J. Ogura, H. Wakai , and H. Aoki, SID Symp. Dig. Tech. **28**, 841 (1997).
[5] P. Rudquist, J. P. F. Lagerwall, M. Buivydas, F. Gouda, S. T. Lagerwall, N. A. Clark, J. E. Maclennan, R.-F. Shao, D. A. Coleman, S. Bardon, T. Bellini, D. R. Link, G. Natale, M. A. Glaser, D. M. Walba, M. D. Wand, and X.-H. Chen, J. Mater. Chem. **9**, 1257 (1999).
[6] N. A. Clark, D. Coleman, and J. E. Maclennan, Liq. Cryst. **27**, 985 (2000).
[7] M. J. O'Callaghan, Phys. Rev. E **67**, 011710 (2003).
[8] N. Vaupotič and M. Čopič, Phys. Rev. E **68**, 061705 (2003).
[9] R. Weinstock, *Calculus of Variations* (Dover, New York, 1974).
[10] I. B. R. Z. B. Musevic, *The Physics of Ferroelectric and Antiferroelectric Liquid Crystals* (World Scientific, Singapore, 2000).
[11] D. Armitage, I. Underwood, and S.-T. Wu, *Introduction to Microdisplays* (Wiley, New York, 2006).
[12] K. H. Yang and T. C. Chieu, Jpn. J. Appl. Phys. **28**, L1599 (1989).
[13] T. C. Chieu and K. H. Yang, Appl. Phys. Lett. **56**, 1326 (1990).
[14] M. J. O'Callaghan, M. D. Wand, C. M. Walker, and M. Nakata, Appl. Phys. Lett. **85**, 6344 (2004).
[15] J. E. Maclennan, M. A. Handschy, and N. A. Clark, Liq. Cryst. **7**, 787 (1990).
[16] C. Wang, M. Wand, M. Handschy, and P. J. Bos, Jpn. J. Appl. Phys. **43**, 3479 (2004).
[17] M. J. O'Callaghan, R. Ferguson, and T. Massopust, SID Symp. Dig. Tech. **38**, 1405 (2007).
[18] M. J. O'Callaghan, R. Ferguson, R. Vohra, W. Thurmes, A. W. Harant, C. S. Pecinovsky, Y. Zhang, S. Yang, M. O'Neill, and M. A. Handschy, J. Soc. Inf. Display **17**, 369 (2009).
[19] M. Reznikov, P. J. Bos, and M. J. O'Callaghan, J. Appl. Phys. **107**, 014103 (2010).
[20] S. P. Palto, Phys. Solid State **51**, 1578 (2009).
[21] J. Dijon, in *Liquid Crystals, Applications and Uses*, edited byB. Bahadur (World Scientific, Singapore, 1990), Vol. 1.
[22] K. H. Yang, T. C. Chieu, and S. Osofsky, Appl. Phys. Lett. **55**, 125 (1989).
[23] S. P. Palto, Crystallogr. Rep. **48**, 124 (2003).
[24] T. Carlsson, N. A. Clark, and Z. Zou, Liq. Cryst. **15**, 461 (1993).
[25] M. J. O'Callaghan, R. Ferguson, R. Vohra, W. Thurmes, A. W. Harant, C. S. Pecinovsky, Y. Zhang, S. Yang, M. O'Neill, and M. A. Handschy, SID Symp. Dig. Tech. **39**, 232 (2008).
[26] S. Kondoh, S. Kawada, R. Takahashi, and E. Tajima, Ferroelectrics **246**, 121 (2000).
[27] M. Terada, S. Yamada, K. Katagiri, S. Yoshihara, and J. Kanbe, Ferroelectrics **149**, 283 (1993).
[28] Q. Jiang, J. E. Maclennan, and N. A. Clark, Phys. Rev. E **53**, 6074 (1996).
[29] Z. Zou, N. A. Clark, and T. Carlsson, Jpn. J. Appl. Phys. **34**, 560 (1995).
[30] Z. Zou and N. Clark, Phys. Rev. Lett. **75**, 1799 (1995).
[31] Z. Zou, N. A. Clark, and M. A. Handschy, Ferroelectrics **121**, 147 (1991).
[32] B. Maximus, E. De Ley, A. De Meyere, and H. Pauwels, Ferroelectrics **121**, 103 (1991).
[33] K. Neyts and F. Beunis, Ferroelectrics **344**, 255 (2006).
[34] K. Neyts, S. Vermael, C. Desimpel, G. Stojmenovik, A. R. M. Verschueren, D. K. G. de Boer, R. Snijkers, P. Machiels, and A. van Brandenburg, J. Appl. Phys. **94**, 3891 (2003).